

Word Instructions and Examples for Creating Version 2 of Your Revised Paper for Screening of Legibility and Length

Two-Column Format with Figures and Tables at the End

Contents:

- Step-by-step instructions for reformatting a Word document and determining length2
- Summary of format specification.....12
- Example formatted paper14

NOTE: The summary of format specifications (pp. 12-13) may be useful to users of word processing software other than Word. Word users are advised to rely on the step-by-step instructions.

Steps for Converting a Word Document into Proper Format for Screening of Figure Legibility and Paper Length by the Combustion Institute

These step-by-step instructions are designed to allow an average Word user to reformat a paper, while avoiding some potential problems with Word. **An average Word user should be able to reformat a paper in about one hour.** This task will be easier if the original Author instructions for submitted papers were followed. Authors should apply those instructions BEFORE reformatting. Format need not be perfect to judge length and figure legibility.

Authors who determine that their paper is too long may want to consider shortening the column-formatted version and then converting a copy of this shortened paper to the double-spaced, single-column format required by Elsevier. This may save time if there are extensive revisions.

Details will depend on the version of Word. Windows shown here are from Word XP.

If you have problems with this reformatting process that cannot be resolved locally, contact Robert Barlow, Sandia National Laboratories, (barlow@ca.sandia.gov).

1. **Print these Instructions (pages 2-11 of this pdf file).**

2. **Make sure you preserve a copy of the original paper (Version 1).**

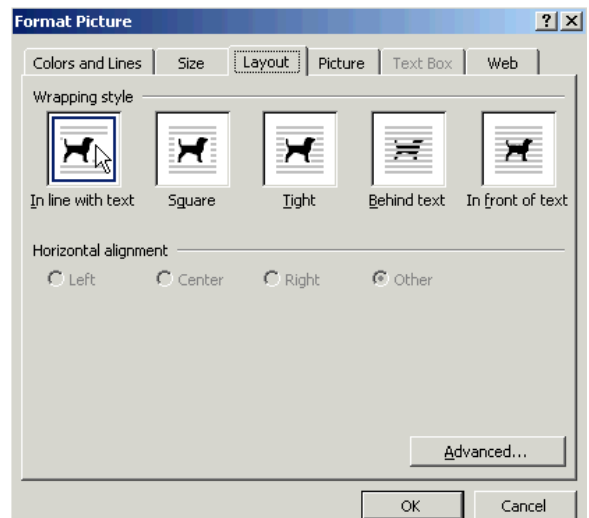
3. Save a copy of your paper, naming the file with your paper ID number followed by “-formatted.” (For example. Save As: **PID12345-formatted.doc**)

4. Place Tables and Figures at the end of the paper with a Page Break before the first table or figure.

5. Format each figure to be “In line with text.”

Double-click on the figure to show the Format Picture command window or go to “Picture ...” under the Format menu. Click on the Layout tab and select “In line with text”. Click OK.

Align each figure on the left margin (align left) as opposed to centered on the page.

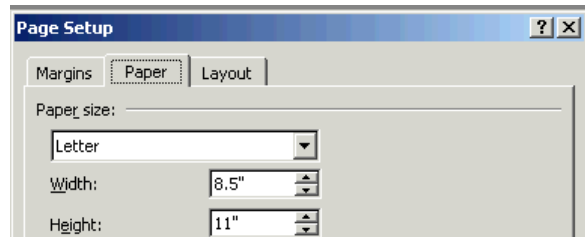


6. Place each figure caption under the corresponding figure. Skip a line between figure and caption, and leave a blank line after each caption.

7. Delete all information that will not be included in the formatted version. Consult the example for what to include.

- a. Delete extra Cover page information.
- b. If there is a separate list of figure captions, delete it, or move it to a separate page at the end of the document.

8. Set the page Type to **US Letter** (8.5in by 11 in).
Use Page Setup...under the File menu.



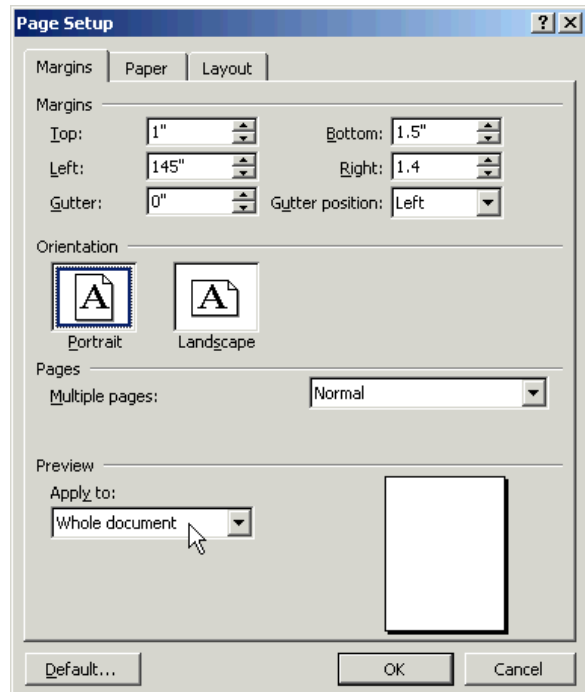
9. Set the margins to:

Top = 1.0 in (25.4 mm)	Bottom = 1.5 in (38.1 mm)
Left = 1.45 in (36.8 mm)	Right = 1.4 in (35.6 mm)

Select "**Apply to: Whole document**"

Click OK.

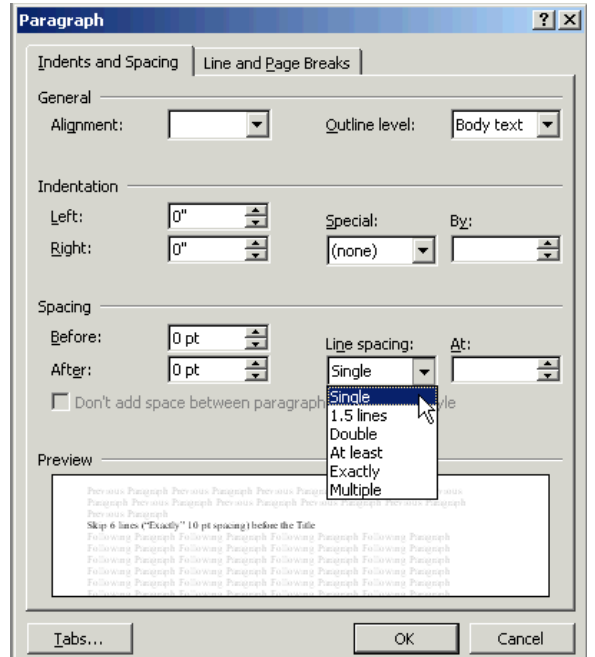
This creates a **printed area** of 8.5-inch (216 mm) in height by 5.65 inch (144 mm) in width. Alternative paper size and margins may be used, as long as this printed area is preserved.



10. Select the entire document. Use [Ctrl-A] or Select All under the Edit menu.

11. Go to “Paragraph...” under the Format menu and apply Single line spacing to the entire document.

Click OK.



12. Insert blank (skipped) lines as listed:

- a. **Six** before the title
- b. One between Title and Authors
- c. One between Authors and Affiliations
- d. **Five** between Affiliations and Abstract
- e. One between Abstract heading and text
- f. One before the Keywords
- g. **Five** between Keywords and Introduction (or first section heading)
- h. One before and after each major heading and each subheading
- i. One before each sub-subheading (if used). Do not skip a line after a sub-subheading.

13. Remove any blank (skipped) lines between paragraphs of text within the Abstract or body of the paper.

14. Remove any blank (skipped) lines between references.

15. Select the complete text from the first line of the file to the final line of the references.

Click the cursor at the beginning of the file,

Scroll to the end of the text, and then

[Shift-Click] after the last reference.

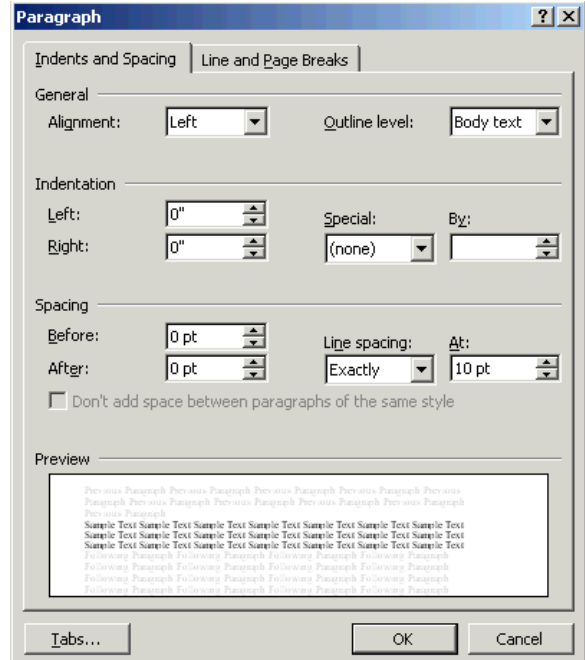
16. With the **entire text** selected (highlighted), set the paragraph line spacing to “Exactly” 10 pt.

Go to “Paragraph...” under the Format menu.

Click OK.

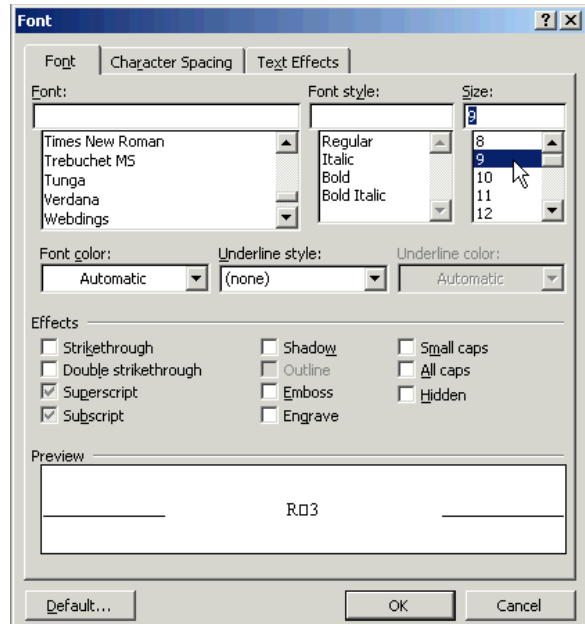
Note that this will squash equations to 10 pt height, but we will switch those back to single line spacing later.

Note that 9 pt font and 10 pt line spacing (9/10) is the most common format, so it is efficient to apply it to all the text and then reformat the special cases.



17. With the **entire text** still selected, set font size to 9 pt. Go to “Font...” under the Format menu.

Click OK.

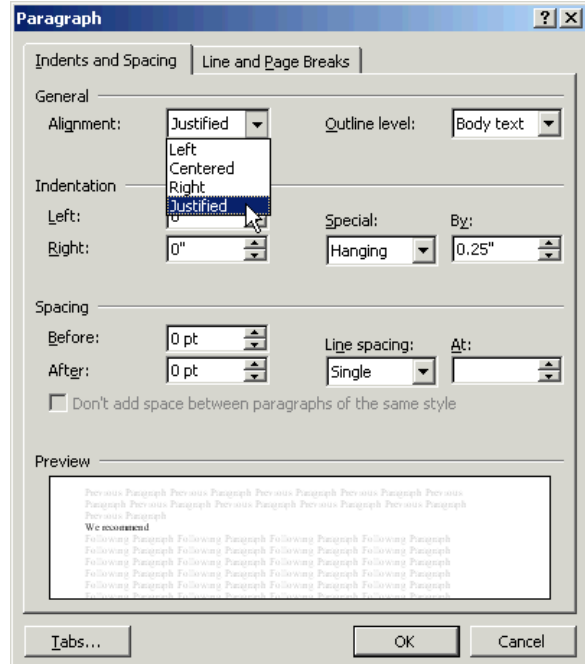
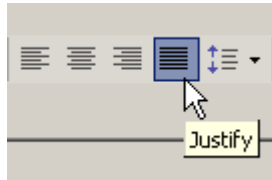


18. Make sure that all sections from the Abstract through the References are justified. (right and left).

Select the text from the abstract to the end of the references.

- a. Click the cursor on a blank line below the author affiliations,
- b. Scroll to the end of the reference list, and then
- c. [Shift-Click] at the end of the references.

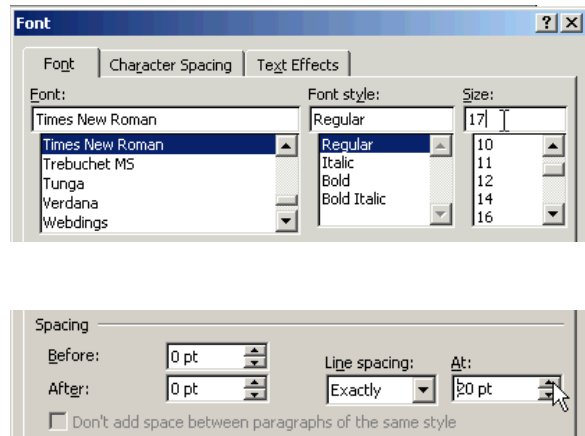
Go to “Paragraph...” under the format menu (at right) or click on the “Justify” button.



19. Select the Article Title and set to (17/20) 17 pt font and “Exactly” 20 pt line spacing.

Use the same “Paragraph...” and “Font...” commands under the Format menu as were used in steps 15 and 16.

Type “17” into the “Size” window.



20. Set the Author Names to (13/15) 13 pt font and 15 pt line spacing

21. Set Author Affiliations to (8/10) *italics*; 8 pt font with Exactly 10 pt line spacing.

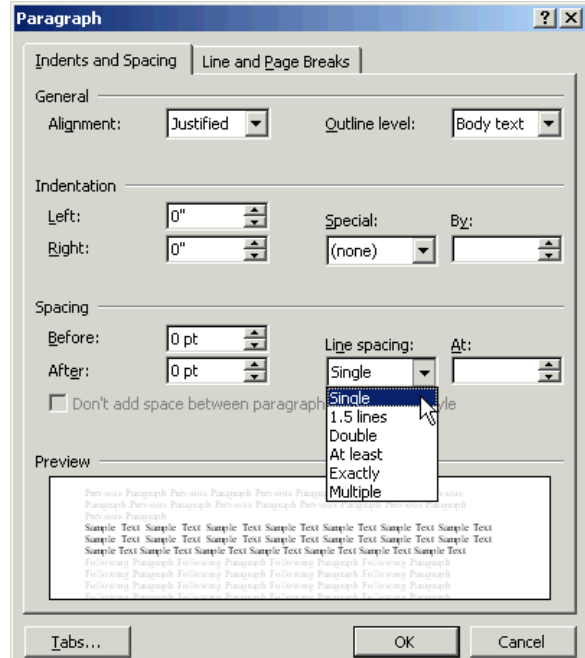
22. Set Keywords to (8/10), 8 pt font with Exactly 10 pt line spacing.

23. Set each equation line to Single line spacing.

Select the one line that contains each equation and go to “Paragraph...” under the Format menu. Change line spacing to Single.

Click OK.

Note: It may be difficult to identify some equation lines at the 10 pt line spacing, so authors should compare to their unformatted version to ensure that all equations appear properly in the formatted version.



24. Select the reference list (not including the Reference heading) and set to (8/9) 8 pt font with “Exactly” 9 pt line spacing.

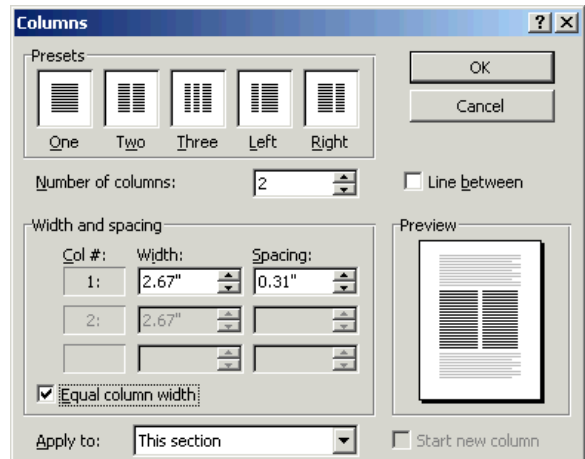
25. Select each Table (all lines) and set to (8/9) 8 pt font with “Exactly” 9 pt line spacing..

26. Select each figure caption and set to (8/9) 8 pt font with “Exactly” 9 pt line spacing..

27. Select all the text for the body of the paper, from the Introduction to the end of the References.

- Go to “Columns...” under the Format menu. Set “Number of columns” to 2.
- Check the box for “Equal column width”
- Enter 2.67”(67.7 mm) for width (spacing will adjust itself to match).

At this stage the text should be properly formatted, and the Tables and Figures remain.
Do not apply two-column format to figures and tables.



28. Size each single column figure such that the **edges of the printed image** extend to a width of 2.67 inch (67 mm).

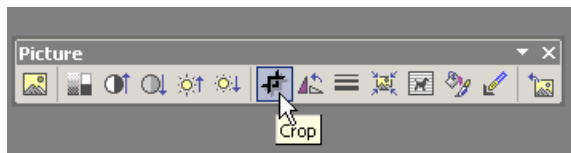
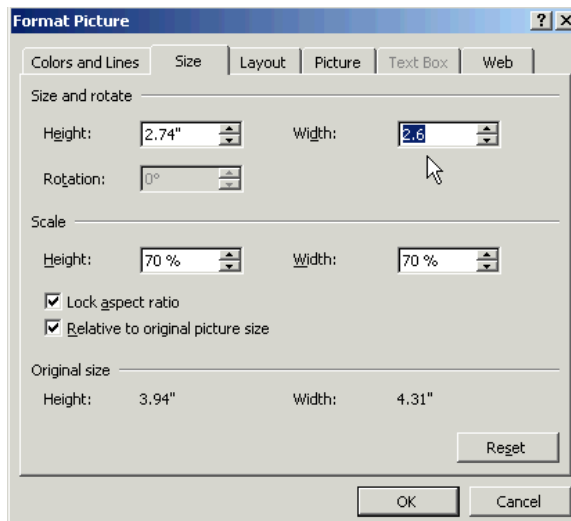
Double-click on the figure to show the Format Picture command window or go to “Picture ...” under the Format menu.

Check the box to “Lock aspect ratio.”

Enter 2.67” (67 mm) for width, **or larger if needed to have the printed part of the figure extend to the full column width**. Click OK.

Alternatively, single-click on the figure and drag the corner to adjust the size.

Note: Excess white space around each figure border should be minimized before setting the image size to fill the column width. This may be done using the “Crop” tool.



29. Size each double column figure such that the **edges of the printed image** extend to a width of 5.5 in (140 mm). Note that this is slightly less than the full page width.

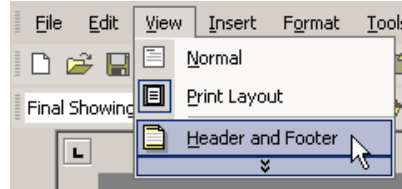
Again, extra white space around the edge of each figure should be minimized.

30. Adjust tabs or table cell widths, as needed, so that each Table fits properly in single-column or full width format.

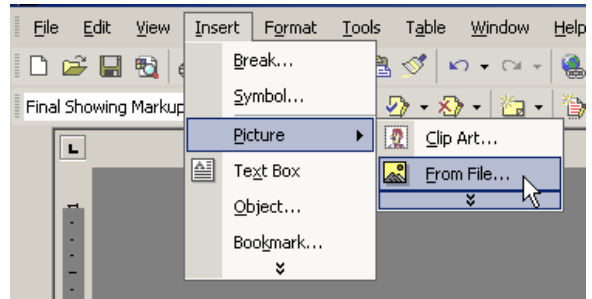
31. The few next steps insert an image of the column boundaries and line numbers behind the formatted paper. This will allow authors and the Combustion Institute personnel to quickly confirm proper formatting and length.

Download the file “**PCI Column Format.jpg**” from the 30th Combustion Symposium site, if you have not already done so.

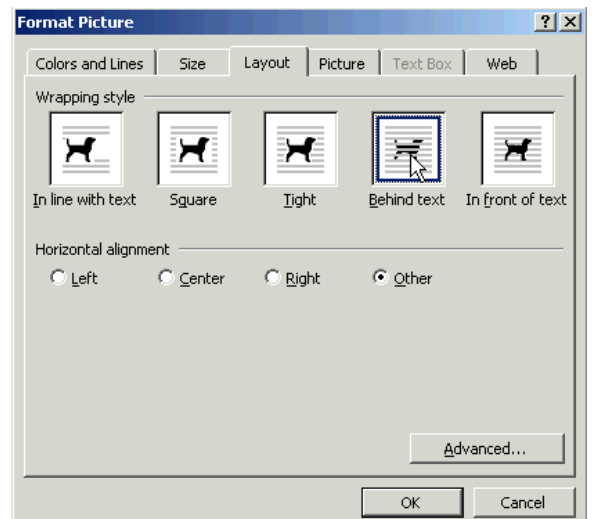
32. Scroll to the first page of the document and click anywhere on the page.
33. Open the Header and Footer under the View menu.



34. Delete any existing text in the header.
35. Insert the image “PCI_Columns.jpg” into the header.
Insert... Picture... From File...



36. Format the Layout to be “Behind text” and 100% size.
- Double click on the image to open the “Format Picture” window or got to “Picture ...” under the Format menu.
- With the Format Picture window still open, click on the “Size” tab and confirm that the image is 100% for both height and width.
- Click OK.

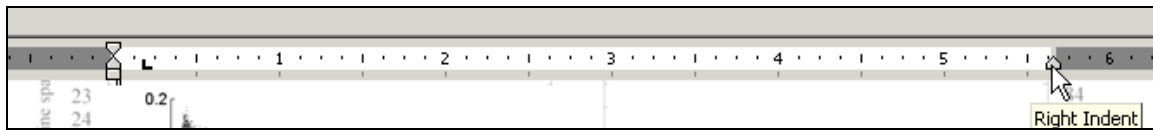


37. Drag the image or use the cursor arrow keys to align the image with the formatted columns. Alignment does not need to be exact. (Word prefers to align the image on its own grid.)
- Close the Header and Footer.
- This should place the column boundary image behind each page of the document.

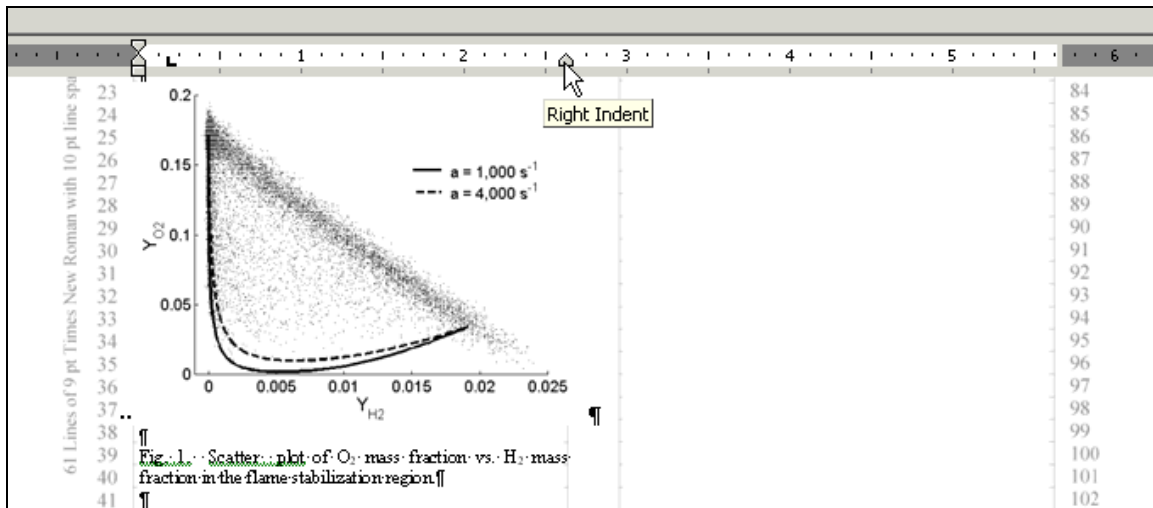


38. We recommend that authors **do not apply two-column format to tables and figures** unless they are fluent with Word and are not using any full width tables or figures.
- Generally, it will be simpler to leave the one-column format in place and adjust the “right indent” on each figure caption to the 2.67-inch width. (See next step.)

39. For **each single-column figure caption**, click within the caption, and then move the “right-indent” marker to match the 2.67 in width (or to the closest increment).



Drag the “Right indent” marker.



40. Add page breaks as needed to prevent figure and caption from being separated.

41. **Save the document.** This completes the formatting process.

Make sure that the file name is of the form **PID12345-formatted.doc**.

42. **Print the file.**

43. **Check that all figures are legible.** A common problem with figures in the submitted Symposium papers is **illegibility of labels, legends, and plotting symbols** due to the use of fonts or symbols that are too small.

Authors should correct any legibility problems before attempting to submit their paper. Papers will not be accepted for publication in the *Proceedings of the Combustion Institute* until all figures are legible at the reduced size.

Note that the resolution used for figures in the CD version of the Proceedings is relatively course compared to a laser printed version. Figures must be easily legible in print if they are to maintain legibility in the final electronic version.

44. Calculate the page equivalent length of the paper.

The maximum allowed length is 7-1/3 pages. This reserves 2/3 page for Comments in the final Proceedings. The equivalent page length of this formatted paper should be determined by adding together the full and partial pages.

Partial pages are measured in terms of column length in units of inches, mm, or 10-pt lines.

To determine page equivalent length:

- a. Count the number of full text pages.
- b. Determine the total column length used on all the partial pages.
Sum the lengths of the partial columns on each page. This may be done in units of inches (8.5 inch total column height), mm (216 mm total column height), or lines (61 total 10-pt lines). Multiply by 2 for double column tables and figures.
- c. Convert the partial columns to equivalent pages. Divide the result in b. by:
(17 column inches/page) or
(432 column mm/page) or
(122 column lines/page)
- d. Combine the number of total and partial pages. If the sum is greater than 7-1/3 pages, the paper **MUST be shortened BEFORE it is submitted.**

45. Convert the reformatted file **to PDF** for upload along with your cover letter to the Colloquium Co-Chair.

- a. **Embed all fonts** in the pdf file.
- b. **View and print** the pdf file to ensure that figures are legible.
- c. The upload URL is given on the Author Checklist

If you have problems with this reformatting process that cannot be resolved locally, contact Robert Barlow, Sandia National Laboratories, (barlow@ca.sandia.gov).

Combustion Institute Format for Figure Legibility and Paper Length
(Use Times New Roman font. Numbers in parentheses give font size and line spacing.)

61 Lines of 9 pt Times New Roman with 10 pt line spacing

1	Skip 6 lines (10 pt line spacing) before the Title	62
2		63
3		64
4		65
5		66
6		67
7		68
8		69
9		70
10		71
11	Skip 1 line (10 pt spacing)	72
12		73
13	Skip 1 line (10 pt spacing)	74
14		75
15		76
16		77
17		78
18	Skip 5 lines (10 pt spacing)	79
19		80
20		81
21	Abstract (bold) (9/10)	82
22		83
23	Text of Abstract (9/10) justified. Use 9 pt times Roman font with "Exactly" 10 pt line spacing in the text of	84
24	the Abstract. Skip one 10 pt line after the Abstract heading. The Abstract runs the full width of two columns.	85
25	Indent paragraphs by 0.17 inch (or similar). The Abstract should contain between 200 and 300 words. Do not	86
26	skip a line between paragraphs.	87
27		88
28	<i>Keywords: (8/10)</i>	89
29		90
30		91
31	Skip 5 lines (10 pt spacing)	92
32		93
33		94
34	1. Introduction (bold) (9/10)	95
35		96
36	Body of text (9/10) justified. Use 9 pt font with	97
37	10 pt line spacing. Main section headings should be	98
38	numbered and in bold face. Skip one line after a	99
39	major heading. Do not skip a line between	100
40	paragraphs. Indent paragraphs by 0.17 in (or	101
41	similar).	102
42	Headings for Nomenclature, Acknowledgments,	103
43	and References are not numbered.	104
44		105
45	<i>1.1 Subheading</i>	106
46		107
47	Sub headings are numbered as above and set in	108
48	italics. Skip one line before and after subheadings.	109
49		110
50	<i>1.1.2 Sub-subheading</i>	111
51	Sub-subheadings, if used, should be numbered	112
52	shown. Do not skip a line after a sub-subheading.	113
53		114
54	2. Page and Column Dimensions	115
55		116
56	Printed page area is 5.67 in by 8.5 in (144 mm by	117
57	216 mm). Column width is 2.67 in (67.7 mm).	118
58	There are 61 lines of 10 pt spacing per column. Note	119
59	that the dimensions of this page may be reduced	120
60	slightly when printed, depending of settings in the	121
61		122

Article Title (17/20)
Article Title (continued)

Author Names (13/15)

Author Affiliations (8/10)

Affiliations (continued) Type one complete affiliation/address per line.

Achrobat printer setup.

References (bold) (9/10)

- [1] Use 8 pt font with 9 pt line spacing (8/9) in the list.
- [2] Number in order of appearance in the text.
- [3] Indent the list by 0.25 inch or equivalent.

Tables

Place all tables and figures at the end of the paper. Use 8 pt font with 9 pt line spacing for Tables and Figure captions. Place figure captions below their respective figures. Do not include a separate list of figure captions in this version.

Include one blank line before and after each table or figure and one blank line between a figure and its caption.

Figures

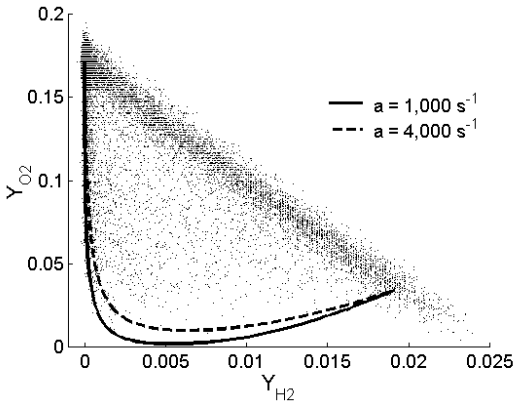
Figures should be sized and aligned such that the outer edge of the printed material extends close to the column boundaries. Single column figures should be sized so that the printed material fills the width of the column. Double column figures may be sized to a width of 5.5inch, (140 mm).

Combustion Institute Format for Figure Legibility and Paper Length
(Use Times New Roman font. Numbers in parentheses give font size and line spacing.)

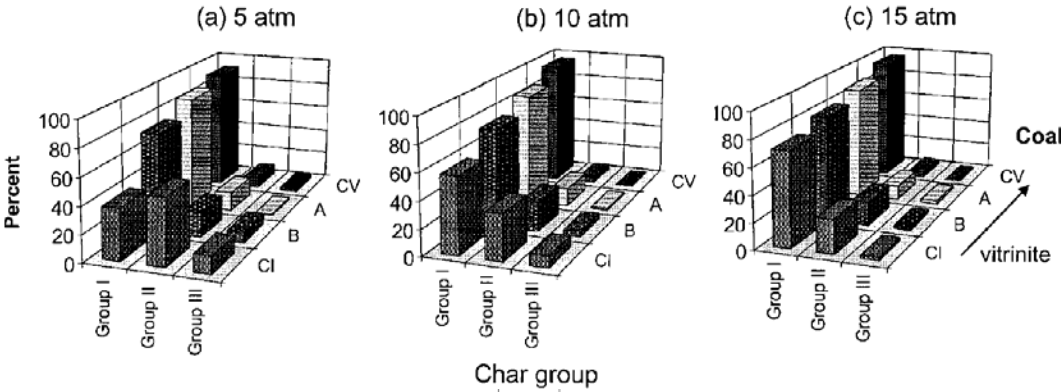
1 Table 1 (8/9)
2 Parameters of the velocity field at the time when the
3 scalars are initialized

Simulation	u'/l	$l/\eta\kappa$	Re_λ	Re_l	N	$k_{max}/\eta\kappa$
R2	1.015	27.2	32	78	256^3	3.88
R3	1.010	42.2	52	153	256^3	2.50
R4	1.005	71.5	72	308	512^3	2.95
R5	1.016	122.6	104	626	512^3	1.75

4
5
6
7
8
9 u'/l , initial large eddy strain rate; $l/\eta\kappa$, initial length-scale
10 ratio; Re_λ , initial Taylor Reynolds number.



11
12
13
14
15
16
17
18
19
20
21
22
23
24
25
26
27 Fig. 1. Scatter plot of O₂ mass fraction vs. H₂ mass
28 fraction in the flame stabilization region.



29
30
31
32
33
34
35
36
37
38
39
40
41
42
43
44
45
46 Fig. 2. Example 2 column figure used in the Author Instruction for submitted papers (from Proc. Combust. Inst. 28, p2235).

61 Lines of 9 pt Times New Roman with 10 pt line spacing

1
2
3
4
5
6
7
8
9
10
11
12
13
14
15
16
17
18
19
20
21
22
23
24
25
26
27
28
29
30
31
32
33
34
35
36
37
38
39
40
41
42
43
44
45
46
47
48
49
50
51
52
53
54
55
56
57
58
59
60
61

62
63
64
65
66
67
68
69
70
71
72
73
74
75
76
77
78
79
80
81
82
83
84
85
86
87
88
89
90
91
92
93
94
95
96
97
98
99
100
101
102
103
104
105
106
107
108
109
110
111
112
113
114
115
116
117
118
119
120
121
122

61 Lines of 9 pt Times New Roman with 10 pt line spacing

Measurements of scalar dissipation in a turbulent piloted methane/air jet flame

Adonios N. Karpetis, Robert S. Barlow*

Combustion Research Facility, Sandia National Laboratories, Livermore, CA 94551-0969, USA

Abstract

This paper describes the first results from a new experimental facility that combines line-imaging measurements of Raman scattering, Rayleigh scattering, and laser-induced CO fluorescence. Simultaneous single-shot line measurements of major species, temperature, mixture fraction, and the radial component of scalar dissipation are obtained in partially premixed methane/air jet flames (25% CH₄, 75% air, by volume). The experimental set up and methods of data analysis are described. Results from a laminar jet flame and a piloted turbulent flame (Sandia flame D) are presented. The laminar and turbulent flames both show a local minimum in the average scalar dissipation near the stoichiometric mixture fraction. In the turbulent flame the radial component of the instantaneous scalar dissipation near the stoichiometric condition displays a log-normal distribution at high values and an exponential distribution at low values. This is attributed to variation in the orientation of the three-dimensional mixture fraction gradient relative to the one-dimensional measurement. The effect of scalar dissipation on flame structure is examined, based on average species mass fractions doubly conditioned upon mixture fraction and scalar dissipation. The length scale of fluctuations in mixture fraction in the turbulent reaction zone is derived from the measured single-shot radial profiles at each streamwise location. This macro length scale is well resolved by the present methods, shows correlation over radial distances of a few millimeters, and grows with streamwise distance as the jet flame spreads. The length scale for fluctuations in scalar dissipation is less than one millimeter at each of the measured streamwise locations in the turbulent flame.

Keywords: Turbulent flames; Scalar dissipation; Raman scattering

1. Introduction

Scalar dissipation is a central concept in the theory and modeling of turbulent nonpremixed and partially premixed flames [1]. There is a need for experimental data on scalar dissipation in hydrocarbon flames that can support the development and validation of improved combustion models. For example, comparisons of measured and modeled results for partially premixed methane/air jet flames [2,3] have shown that conditional moment closure (CMC) and steady flamelet models, each of which depend on a submodel for conditional scalar dissipation, over predict the progress of reaction in fuel-rich conditions. It is known from studies of laminar partially premixed flames that reaction

progress in fuel-rich conditions is sensitive to the applied strain or scalar dissipation rate. Therefore, accurate modeling of scalar dissipation is expected to be especially important for partially premixed turbulent flames, making them good candidates for the present experiments. Pitts et al. [4] provide a review of scalar dissipation measurements in nonreacting jets. Measurements in turbulent flames are more limited because scalar dissipation, defined as $\chi = 2D_\xi (\nabla \xi \cdot \nabla \xi)$, where ξ is the mixture fraction and D_ξ is its diffusivity, is obtained from the spatial derivative (in at least one dimension) of the mixture fraction, which is difficult to measure accurately in flames on a single-shot basis with good spatial resolution. Nandula et al. [5], Chen & Mansour [6], and Brockhinke et al. [6] used KrF

1 excimer lasers and intensified CCD arrays to obtain
2 single shot measurements of the radial component of
3 scalar dissipation in turbulent H₂ jet flames.
4 Methane flames present a greater challenge [7-10]
5 because laser excited fluorescence of higher
6 hydrocarbons interferes with Raman scattering
7 measurements. While line imaging of Raman
8 scattering has been applied in turbulent nonpremixed
9 hydrocarbon flames [11], we are not aware of any
10 published results on scalar dissipation from such
11 measurements. There is ongoing work to develop
12 techniques for two-dimensional measurements of
13 mixture fraction in methane flames [12-14].
14 However, the measurement of all the major species,
15 which should yield the best accuracy in mixture
16 fraction, is currently practical only in the context of
17 line imaging. This paper presents the first results
18 from a facility that combines line imaging of Raman
19 scattering, Rayleigh scattering, and laser-induced CO
20 fluorescence to obtain measurements of temperature,
21 the major species concentrations, mixture fraction,
22 and scalar dissipation in turbulent hydrocarbon
23 flames. Temporally resolved measurements were
24 obtained along radial segments in a piloted CH₄/air
25 jet flame (Sandia flame D [2,15]) and in a laminar jet
26 flame (flame A [15]) with the same fuel composition
27 of 25% CH₄ and 75% air, by volume.

28 29 **2. Experimental Methods**

30 31 *2.1 Line-Imaging Raman/Rayleigh/LIF system*

32
33 The experimental set up is shown in Fig. 1. Four
34 frequency-doubled Nd:YAG lasers were used in the
35 Raman/Rayleigh system. Dichroic optics
36 successively combined each frequency-doubled
37 beam (532 nm) with the 1064 nm beam of the next
38 laser in the series, before it passed through the
39 doubling crystal. Collimating telescopes in three of
40 the lasers allowed for matching of the waists of the
41 four beams. Dielectric breakdown in the probe
42 volume was avoided by separating the pulses in time
43 by 200 ns and by using a three-leg pulse stretcher,
44 which extended each pulse to about 80 ns (FWHM).
45 The combined beam was focused into the test section
46 using a 500 mm lens. Alignment of the multiple
47 beams was accomplished using seven motor-driven
48 mirror mounts, one for each laser and one in each leg
49 of the pulse stretcher. The pulse energy was
50 measured using a thermoelectric Joule-meter. Due
51 to hardware problems, the present experiments were
52 conducted using roughly 0.9 J/pulse out of the 2.4
53 J/pulse that the system can deliver to the probe
54 volume. Excitation of CO followed the methods
55 developed for multiscalar point measurements at
56 Sandia [e.g. 3]. A seeded Nd:YAG laser pumped a
57 tunable dye laser, and the dye laser beam was
58 frequency doubled and then mixed with the Nd:YAG
59 fundamental to reach 230 nm. Laser pulse energy
60 was measured using a photodiode, and the
61 combination of a $\lambda/2$ plate and Glan laser prism was

used to attenuate pulse energy and maintain it in the
range (~1.5 mJ/pulse) that yielded a nearly linear
dependence between laser energy and CO
fluorescence signal along the length of the imaged
region. This reduces the influence of collisional
quenching [3], and corrections for variation in the
quenching rate were not applied.

Raman scattered light was collected using a
custom designed pair of 150-mm diameter achromats
(Linos Photonics, $f/2$ and $f/4$), which were mounted
face to face, yielding a magnification of 2. The $f/4$
lens matched the entrance aperture of an imaging
spectrometer, which was fitted with a high-speed
rotating mechanical shutter [9,16,17]. This shutter
provided a 9 μ s gate, rejecting flame luminosity and
allowing the use of a non-intensified CCD array
detector. The shutter also provided timing signals
for the lasers and cameras.

A 16-bit, back-illuminated, cryogenically-cooled
CCD (Princeton Instruments VersArray 1300B with
1300x1340 pixels) was used for detection of the
Raman spectrum. The performance of such cameras
is superior to that of intensified cameras, with regard
to quantum efficiency, noise, and dynamic range, as
described by Miles [16]. The image of the laser
beam was rotated by a periscope to align with the
vertical entrance slit. A grating of 588 grooves/mm
dispersed the Stokes Raman spectrum (550–700 nm)
along the horizontal axis of the CCD detector. The
diameter of the probe volume was determined by the
~250 μ m waist of the combined laser beam, the
image of which (500 μ m after magnification) fits
through the 800 μ m rotating slit. In order to
minimize readout noise and hence improve the
overall signal-to-noise ratio (SNR), CCD pixels were
binned on chip to form superpixels. For the present
experiment 23 superpixels were defined along the
spatial dimension of the CCD, corresponding to a
spatial resolution of 300 μ m along the laser beam,
and 15 superpixels were defined along the spectral
dimension. The CCD detector allowed for arbitrary
specification of the location and width of superpixel
columns, and these spectral superpixels collected
photons corresponding to the rotational-vibrational
Raman spectrum of the major species (CO₂, O₂, CO,
N₂, CH₄, H₂O, H₂) and interferences in-between.

The Rayleigh imaging system used two matched
achromats (82 mm diameter, 300-mm fl, 1:1
conjugation), and the collected light was focused
onto a back-illuminated CCD detector (Roper
Scientific Spec-10 400B with 400x1340 pixels)
through a 532-nm band-pass filter. Gating was
provided by a mechanical shutter and a ferro-electric
liquid crystal shutter. The horizontal image was
divided into 23 superpixels of 300 μ m, matching the
Raman system. The vertical image was divided into
15 pixels of 60 μ m, with upper and lower pixel rows
being used for shot-to-shot subtraction of
background scattering.

The CO imaging system used the same front
collection lens as the Rayleigh system. A dichroic

62
63
64
65
66
67
68
69
70
71
72
73
74
75
76
77
78
79
80
81
82
83
84
85
86
87
88
89
90
91
92
93
94
95
96
97
98
99
100
101
102
103
104
105
106
107
108
109
110
111
112
113
114
115
116
117
118
119
120
121
122

1 beam splitter in the collimated region reflected CO
 2 fluorescence from the $B^1\Sigma^+(v''=0)\rightarrow A^1\pi(v'=1)$ band
 3 (~484 nm) through another matched achromat. An
 4 interference filter centered at 484 nm (10 nm
 5 FWHM) passed the CO fluorescence signal onto an
 6 intensified CCD camera (Andor) with 512x512
 7 pixels. As for the other systems, the imaged region
 8 was divided into 23 superpixels along the length of
 9 the laser beam. Seven superpixels were used in the
 10 vertical direction, with the outer pixels again being
 11 used for background subtraction.

12 2.2. Data analysis

13 Processing steps for the Raman, Rayleigh, and
 14 CO LIF images included: dark frame subtraction,
 15 correction for non-uniform throughput and response
 16 of each imaging system, background subtraction, and
 17 normalization by laser energy. The signals from
 18 each superpixel element were then converted to
 19 scalar quantities using an iterative matrix inversion
 20 process similar to that developed for point
 21 measurements [e.g. 3,8]. Diagonal elements of the
 22 matrix include a calibration factor and a temperature
 23 dependent bandwidth function for each species. Off-
 24 diagonal elements account for the temperature-
 25 dependent cross-talk among species and the effects
 26 of laser-excited interferences. Here we have used
 27 the signal from the C_2 band near 560 nm, rather than
 28 the band near 615 nm, to correct for interferences.
 29 (The 560-nm signal is stronger and less affected by
 30 cross-talk from CH_4 .) The major species mole
 31 fractions from the Raman/LIF measurements were
 32 used to determine the species-weighted Rayleigh
 33 scattering cross section, and the resulting Rayleigh
 34 temperature was iteratively applied in calculating the
 35 temperature dependent matrix elements, until
 36 convergence to <1K was achieved. The LIF
 37 technique is superior to Raman scattering for the
 38 measurement of CO in methane flames [8,18], and
 39 LIF results for CO are used exclusively in this paper.

40 Mixture fraction was calculated from the
 41 measured species mass fractions, Y_i , using the Bilger
 42 formulation [19] modified as in previous work on
 43 these partially premixed flames to exclude the
 44 oxygen terms [3,15]. This reduces sensitivity to
 45 measurement noise and interferences. The mixture
 46 diffusivity was evaluated as:

$$47 D_{\xi} = -0.12013 + 0.74818(T/1000) +$$

$$48 1.1631(T/1000)^2 \text{ (cm}^2/\text{s)}, \quad (1)$$

49 which is a fit to the mixture-averaged diffusivity
 50 from a calculation of an opposed-flow, laminar,
 51 partially premixed CH_4 /air flame with a strain
 52 parameter for the Tsuji configuration of $a=25 \text{ s}^{-1}$ [3].
 53 Two methods for determining the radial derivative of
 54 ξ were investigated, spline smoothing and central
 55 differencing. Results presented here are based on
 56 spline smoothing with the error constraint on mixture
 57 fraction set at $0.005 + 0.005\xi$ to account
 58 for measurement uncertainty. Scalar
 59 dissipation statistics (*pdf* shapes and conditional means) were
 60 relatively insensitive to error constraints between
 61 zero and the level applied here. Central differencing
 yielded scalar dissipation statistics very similar to
 those presented below.

62 approximately for measurement uncertainty. Scalar
 63 dissipation
 64 statistics (*pdf* shapes and conditional means) were
 65 relatively insensitive to error constraints between
 66 zero and the level applied here. Central differencing
 67 yielded scalar dissipation statistics very similar to
 68 those presented below.

69 3. Results and Discussions

70 3.1 Laminar flame results and measurement precision

71 Measurements were obtained in a laminar
 72 partially premixed jet flame (flame A [15]) in order
 73 to evaluate the precision of repeated measurements.
 74 The standard deviation in mixture fraction
 75 measurements (unsmoothed) in this flame varies
 76 from about 5% in lean conditions to 0.9% in very
 77 rich conditions. Standard deviation in the measured
 78 scalar dissipation varies from ~17% to ~30%.
 79 However, this level of precision is still quite useful
 80 in the turbulent flame, where instantaneous χ values
 81 (presented below) are distributed over 3-4 orders of
 82 magnitude. (For simplicity, χ is used in the
 83 remainder of this paper to denote the measured radial
 84 component of scalar dissipation.) The measured
 85 profile of χ in this laminar jet flame has two peaks,
 86 with a local minimum just to the rich side of the
 87 stoichiometric mixture fraction, $\xi_{st}=0.35$.
 88 Calculations of laminar opposed-flow flames [3]
 89 show a similar double-peaked structure. However,
 90 the measurements yield a rich-side peak in scalar
 91 dissipation that is roughly three times that on the
 92 lean side, while the corresponding ratio in the
 93 calculation is less than two. This reflects a
 94 difference in structure between the axisymmetric jet
 95 and opposed-flow configurations. Note that the
 96 shape of the scalar dissipation profile can depend on
 97 how mixture fraction is defined. Therefore,
 98 consistent definitions should be used in such
 99 comparisons.

100 3.2 Scalar dissipation statistics in turbulent flame D

101 Flame D in the series of piloted CH_4 /air jet
 102 flames [15] has been a target of numerous model
 103 calculations [e.g. 2,20-22]. It is an appropriate flame
 104 for this investigation of scalar dissipation because it
 105 has a relatively high Reynolds number, $Re=22,400$,
 106 but a low probability of localized extinction. Line
 107 measurements were obtained at streamwise positions
 108 of $x/d=7.5, 15, \text{ and } 30$. In each case the flame was
 109 aligned so that the imaged segment was
 110 approximately centered on the mean stoichiometric
 111 contour. 1000 shots, the equivalent of 23,000 point
 112 measurements, were acquired at each streamwise
 113 location.

114 Results for the radial component of scalar
 115 dissipation are presented in Fig. 2 as two-
 116 dimensional density plots. These plots are
 117 constructed from one-dimensional probability
 118
 119
 120
 121
 122

1 density functions (*pdf*'s) of scalar dissipation
 2 conditioned upon the mixture fraction, such that each
 3 represented value of ξ (each vertical slice) has equal
 4 probability. As suggested by Chen & Mansour [6],
 5 scalar dissipation is examined in logarithmic space,
 6 hence the presentation of $pdf(\ln\chi|\xi)$. The darker
 7 areas correspond to higher probability. The solid
 8 line in each density plot represents the average value
 9 of scalar dissipation conditioned upon the mixture
 10 fraction, $(\ln\langle\chi|\xi\rangle)$.

11 Scalar dissipation is broadly distributed at all
 12 measured positions in the flame except on the fuel-
 13 lean side close to the exit ($x/d=7.5$), where the flow
 14 field is not fully turbulent. There is a clear trend
 15 towards smaller values of χ with increasing
 16 downstream distance, manifested both in the density
 17 plots and the average values. The streamwise decay
 18 in ξ , manifested in the progressive erosion of very
 19 rich samples, is also evident. The double-peak
 20 structure noted in the laminar jet flame persists in the
 21 turbulent flame. A local minimum in χ can be seen
 22 near the stoichiometric value (marked by a dotted
 23 line in Fig. 2) at all three streamwise locations. The
 24 local maxima in χ are higher on the fuel-rich side of
 25 the flame, which is consistent with previous
 26 measurements [5,6] and LES results [20]. The
 27 values of the conditional average $\langle\chi|\xi\rangle$ at the rich-
 28 side maxima ($\xi\sim 0.5$) are 63, 42, and 16 s^{-1} for
 29 $x/d=7.5, 15, \text{ and } 30$, respectively. The corresponding
 30 local minima (near $\xi_{st} = 0.35$) are 17, 10, and 4 s^{-1} .
 31 Full three-dimensional results for scalar dissipation
 32 are expected to be higher by a factor between 2 and
 33 3.

34 The one-dimensional *pdf* of χ at the
 35 stoichiometric condition, $pdf(\ln\chi|\xi_{st})$, has
 36 significance for both theory and modeling of reacting
 37 flows. Experiments in cold flows [4,23] suggest a
 38 log-normal distribution for this *pdf*, while some
 39 experiments in reacting flows have suggested a
 40 different shape [6]. Here, this *pdf* was generated
 41 from measurements at $x/d=7.5, 15, \text{ and } 30$. A large
 42 bin was selected around the stoichiometric value, as
 43 shown by the lines and arrows in the density plots in
 44 Fig. 2, to provide sufficient statistical accuracy. The
 45 results are shown in the lower graphs in Fig. 2,
 46 where the $pdf(\ln\chi|\xi_{st})$ is plotted in log-arithmetic
 47 ordinate. For each streamwise location the right side
 48 of the *pdf*, corresponding to the high values of χ can
 49 be approximated by a log-normal distribution
 50 (appearing as a parabola in such a plot). The left
 51 side of the *pdf*, corresponding to small values of χ
 52 appears closer to an exponential (and hence a
 53 straight line in each graph). As explained in [24] for
 54 isotropic turbulent flows, the deviation from log-
 55 normality for the smaller values of scalar dissipation
 56 can be considered an artifact of the 1D measurement.
 57 As the instantaneous gradient vector, $\nabla\xi$ deviates
 58 from the radial direction, the 1D technique registers
 59 the projection of the vector along r and consequently
 60 lower values of $\tilde{\chi}$. This can be seen in Fig. 2, where
 61 the deviations from log-normality become more

62 pronounced as distance from the exit increases, and
 63 the flame orientation varies more from the radial.
 64 Future experiments will include simultaneous planar
 65 imaging to determine the instantaneous flame
 66 orientation and curvature.

3.3 Influence of scalar dissipation on species

70 The present measurements allow direct
 71 assessment of the effects of scalar dissipation on
 72 turbulent flame structure and reaction progress.
 73 Instantaneous realizations (not shown here) give
 74 clear illustrations of turbulence-chemistry coupling.
 75 For example, CO levels on the fuel-rich side of the
 76 reaction zone are significantly reduced in single-shot
 77 profiles with high local scalar dissipation. The joint
 78 conditional statistics of mixture fraction, scalar
 79 dissipation, and reactive scalars may be analyzed in
 80 various ways, which we can only begin to address
 81 here. We will approach the issues in the context of
 82 classic ideas that describe a turbulent flame as a
 83 collection of strained laminar flamelets [1]. Every
 84 measurement point (Y_i, ξ, χ) may be considered as a
 85 part of a doubly conditioned flamelet (conditioned
 86 on ξ and χ). The previous section dealt with the
 87 results in the (ξ, χ) plane of the multidimensional
 88 scalar space that describes the turbulent flame. In
 89 what follows, we will consider results in planes of
 90 (Y_i, ξ) and (Y_i, χ) .

91 There are at least two possibilities for calculating
 92 doubly conditioned averages of state variables: one
 93 is to condition upon the local scalar dissipation, χ ,
 94 another is to condition upon the scalar dissipation at
 95 the closest stoichiometric condition, χ_{st} , along the
 96 instantaneous radial segment. The latter is presented
 97 here because it is more consistent with the
 98 theoretical treatment of flamelets, which are
 99 typically described according to the stoichiometric
 100 value of scalar dissipation [1]. Fig. 3 presents results
 101 in the form $\langle Y_i | \xi, \chi_{st} \rangle$ for H_2O , CH_4 , CO , and H_2 .
 102 Data from all three streamwise measurement
 103 locations were combined, and conditioning on χ_{st}
 104 was performed using the five logarithmic intervals
 105 listed in the figure caption. Arrows indicate in the
 106 direction of increasing χ_{st} . Changes in the flamelet
 107 structure appear for the highest values of χ_{st} , and
 108 they are confined around the stoichiometric value, as
 109 anticipated by the conditioning method (upon χ_{st}).
 110 The water mass fraction is representative of
 111 temperature, CO_2 and overall reaction progress and
 112 is shown first. As χ_{st} increases, the local mixing time
 113 ($1/\chi_{st}$) decreases. This translates to a decrease of
 114 local Damköler number and leads to the observed
 115 reduction of $\langle Y_{H_2O} | \xi, \chi_{st} \rangle$ in Fig. 3. A
 116 corresponding effect is seen in the results for
 117 $\langle Y_{CH_4} | \xi, \chi_{st} \rangle$. Higher values of χ_{st} result in
 118 increased leakage of CH_4 across the stoichiometric
 119 condition and into the lean side of the flame. The
 120 intermediates, CO and H_2 , show a more pronounced
 121 effect of scalar dissipation, which is most apparent
 122 on the fuel-rich side, where peak levels of CO and

1 H₂ are reduced as χ_{st} increases. The behavior of
 2 species mass fractions shown in Fig. 3 is the
 3 expected response of flame structure to decreasing
 4 Damköler number [1,25], and it is qualitatively
 5 consistent with results from steady laminar flame
 6 calculations performed over a range of scalar
 7 dissipation rates. The novel contribution of the
 8 present work is that these doubly conditioned species
 9 mass fractions are quantified for the first time in a
 10 turbulent CH₄/air flame.

11 The present measurements also provide
 12 information on the approach to extinction. As an
 13 illustration, we consider the mass fraction of water
 14 conditioned upon the stoichiometric mixture
 15 fraction, ξ_{st} , and the instantaneous stoichiometric
 16 scalar dissipation, χ_{st} . By conditioning on ξ_{st} we
 17 ensure that only the local stoichiometric flamelets
 18 are included in the ensemble. These correspond to
 19 the most vigorous burning condition and the largest
 20 values of local and instantaneous Y_{H_2O} . In Fig. 4 the
 21 doubly conditioned average $\langle Y_{H_2O} | \xi_{st}, \chi_{st} \rangle$ is
 22 plotted against $\log \chi_{st}$. The result corresponds to the
 23 upper burning branch of an S-shaped curve
 24 (mirrored, since we use the abscissa $\log \chi_{st}$ rather
 25 than $\log 1/\chi_{st}$ that corresponds to time). The
 26 approach to extinction is clearly seen by the dip in
 27 $\langle Y_{H_2O} | \xi_{st}, \chi_{st} \rangle$ for values approaching $\chi_{st} \approx 400 \text{ s}^{-1}$.
 28 The curve drawn through the data is a quasi-analytic
 29 prediction of the S-shaped curve for single-step
 30 kinetics and for judicious choice of parameters [26].
 31 It is plotted as a visual aid to indicate the expected
 32 shape of the curve and not for reasons of
 33 comparison, because of the many adjustable
 34 parameters that the model requires. The presence or
 35 absence of localized re-ignition can be judged from
 36 the structure of the instantaneous results at a constant
 37 scalar dissipation, χ_o , below the extinction limit. In
 38 regions having significant extinction and re-ignition
 39 a bi-modal distribution of values $Y_{H_2O} | \xi_{st}, \chi_o$ would
 40 be expected, corresponding to both the upper and
 41 the lower stable branches of the S-shaped curve.
 42 Samples corresponding to the lower (re-ignition)
 43 branch were not observed in the present experiment.

44 3.4 Spatial structure of turbulent flame D

45 Two-point and multi-point spatial correlations of
 46 scalar quantities can be calculated from line
 47 measurements [6], leading to the calculation of
 48 length scales pertinent to turbulent combustion. The
 49 normalized auto-correlation,
 50

$$51 R_{\alpha\alpha}(x, r, \Delta r) \equiv \frac{\langle \alpha'(x, r) \alpha'(x, r + \Delta r) \rangle}{\langle \alpha'^2(x, r) \rangle^{1/2} \langle \alpha'^2(x, r + \Delta r) \rangle^{1/2}} \quad (2)$$

52 may be calculated for any scalar α . The quantity $R_{\alpha\alpha}$
 53 may then be integrated over Δr to produce a length-
 54 scale l_α :

$$55 l_\alpha(x, r) \equiv \int R_{\alpha\alpha}(x, r, \Delta r) d\Delta r \quad (3)$$

56 The length-scales for fluctuations in mixture
 57 fraction ($\alpha \equiv \xi$) and fluctuations in scalar dissipation
 58 ($\alpha \equiv \chi$) have been calculated and are plotted in Fig.
 59 as a function of axial distance, x/d . The former, l_ξ ,
 60 corresponds to a macro-scale of turbulence, while
 61 the latter, l_χ , is characteristic of the length scale
 62 where most scalar dissipation occurs. It should be
 63 noted that the dependence on the radius has been
 64 tacitly suppressed, and the length-scales are
 65 considered representative of the reacting region at
 66 each axial position. The scale l_ξ is well resolved in
 67 this experiment and increases with axial distance as
 68 the flame spreads. However, l_χ is greatest at $x/d=7.5$
 69 and decreases with axial distance. This trend may
 70 result from the transitional character of the flame in
 71 the near field, where combustion suppresses
 72 turbulence. Better spatial resolution, which will be
 73 achieved in future experiments, will be needed to
 74 confirm the quantitative behavior of l_χ , but it is clear
 75 that fluctuations in scalar dissipation are only
 76 correlated over distances of less than 1 mm at these
 77 turbulent flame conditions.

78 4. Conclusions

79 Measurements of the major species mass
 80 fractions, mixture fraction, and the radial component
 81 of scalar dissipation were obtained in laminar and
 82 turbulent methane/air jet flames (flames A and D),
 83 using simultaneous line imaging of Raman
 84 scattering, Rayleigh scattering, and laser-induced CO
 85 fluorescence. Local minima in the conditional scalar
 86 dissipation near the stoichiometric condition are
 87 exhibited by both types of flames. Pdfs of scalar
 88 dissipation conditional upon mixture fraction are
 89 broadly distributed about the conditional mean.
 90 One-dimensional pdfs of the radial component of the
 91 conditional scalar dissipation around the
 92 stoichiometric mixture fraction exhibit log-normal
 93 behavior for high scalar dissipation values but appear
 94 to follow an exponential distribution for low scalar
 95 dissipation values, and this is attributed to variation
 96 in the orientation of the instantaneous three-
 97 dimensional gradient in mixture fraction. Average
 98 species mass fractions, doubly conditioned upon
 99 mixture fraction and scalar dissipation, clearly show
 100 the effects of high scalar dissipation and finite rate
 101 chemistry on flame structure, including the approach
 102 to extinction in the turbulent flame. The length scale
 103 of turbulent fluctuations in mixture fraction across
 104 the reaction zone shows the effect of jet spreading
 105 and shows positive correlation over distances of a
 106 few millimeters. The length scale of fluctuations in
 107 scalar dissipation is less than 1 mm at the three
 108 measured locations in flame D.

109 Acknowledgments

110 This work was supported by the U.S. Department
 111 of Energy, Office of Basic Energy Sciences.
 112 Contributions by R. Schefer, T. Settersten, and P.

61 Lines of 9 pt Times New Roman with 10 pt line spacing

1 Miles toward the development of this new facility
2 and by R. Harmon in support of these experiments
3 are gratefully acknowledged. Insightful suggestions
4 by R. Bilger, A. Kerstein, H. Pitsch, and S. Pope are
5 much appreciated.

6
7 **References**

8
9 [1] N. Peters, *Turbulent Combustion*, Cambridge
10 University Press, Cambridge, 2000.
11 [2] Web site for the TNF Workshop, R.S. Barlow, Ed.,
12 Sandia National Laboratories,
13 <http://www.ca.sandia.gov/tdf/Workshop>.
14 (Proceedings of the TNF3, TNF4, and TNF5
15 Workshops.)
16 [3] R.S. Barlow, R.S. Karpetis, A.N. Frank, J.H., Chen,
17 J.-Y., *Combust. Flame* 127 (2001) 2102-2118.
18 [4] W.M. Pitts, C.D. Richards, M.S. Levenson, *Large
19 and Small Scale Structures and Their Interactions in
20 an Axisymmetric Jet*, NISTIR 6393, NIST, 1999,
21 available at [http://fire.nist.gov/
22 bfrlpubs/fire99/art071.html](http://fire.nist.gov/bfrlpubs/fire99/art071.html).
23 [5] S.P. Nandula, R.W. Pitz, T.M. Brown, *Combust.
24 Flame* 99 (1994) 775-783.
25 [6] Y.-C. Chen, M.S. Mansour, *Combust. Sci. Tech.* 126
26 (1997) 291-313.
27 [7] A. Brockhinke, S. Haufe, K. Kohse-Höinghaus,
28 *Combust. Flame* 121 (2000) 367-377.
29 [8] P.A. Nooren, M. Versluis, T.H. van der Meer, R.S.
30 Barlow, J.H. Frank, *Appl. Phys. B* 71 (2000) 95-111.
31 [9] R.S. Barlow, P.C. Miles, *Proc. Comb. Inst.* 28
32 (2000) 269-278.
33 [10] W. Meier, O. Keck, *Meas. Sci. Tech.* 13 (2002) 741-
34 749.
35 [11] N. Ebersohl, Th. Klos, R. Suntz, H. Bockhorn, *Proc.
36 Comb. Inst.* 27 (1998) 997-1006.
37 [12] S.H. Stårner, R.W. Bilger, M.B. Long, J.H. Frank,
38 D.F. Marran, *Combust. Sci. Tech.* 129 (1997) 141-
39 163.
40 [13] J. Fielding, A.M. Schaffer, and M.B. Long, *Proc.
41 Comb. Inst.* 27 (1998) 1007-1014.
42 [14] J.H. Frank, S.A. Kaiser, M.B. Long, *Proc. Comb.
43 Inst.* 29 (2002) 2687-2694.
44 [15] R.S. Barlow, J.H. Frank, *Proc. Comb. Inst.* 27
45 (1998) 1087-1095.
46 [16] P.C. Miles, *Appl. Optics* 38 (1999) 1714-1732.
47 [17] P.C. Miles, R.S. Barlow, *Meas. Sci. Tech.* 11 (2000)
48 392-397.
49 [18] W. Meier, R.S. Barlow, Y.L. Chen, J.-Y. Chen,
50 *Combust. Flame* 123 (2000) 326-343.
51 [19] R.W. Bilger, S.H. Stårner, R.J. Kee, *Combust.
52 Flame* 80 (1990) 135-149.
53 [20] H. Pitsch, H. Steiner, *Proc. Comb. Inst.* 28 (2000)
54 41-50.
55 [21] Q. Tang, J. Xu, S.B. Pope, *Proc. Comb. Inst.* 28
56 (2000) 133-140.
57 [22] R.P. Lindstedt, S.A. Louloudi, E.M. Vaos, *Proc.
58 Comb. Inst.* 28 (2000) 149-156.
59 [23] K. Sardi, A.M.K.P. Taylor, J.H. Whitelaw, *J. Fluid
60 Mech.* 361 (1998) 1-24.
61 [24] W.J.A. Dahm, K.A. Buch, *Phys. Fluids A* 1 (1989)
1290-1293.
[25] R.S. Barlow, G.J. Fiechtner, C.D. Carter, J.-Y. Chen,
Combust. Flame 120 (2000) 549-569.
[26] H. Pitsch, S. Fedotov, *Combust. Theory Modelling* 5
(2001) 41-57.

5 full pages + 60 lines.

	62
	63
	64
	65
	66
	67
	68
	69
	70
	71
	72
	73
	74
	75
	76
	77
	78
	79
	80
	81
	82
	83
	84
	85
	86
	87
	88
	89
	90
	91
	92
	93
	94
	95
	96
	97
	98
	99
	100
	101
	102
	103
	104
	105
	106
	107
	108
	109
	110
	111
	112
	113
	114
	115
	116
	117
	118
	119
	120
	121
	122

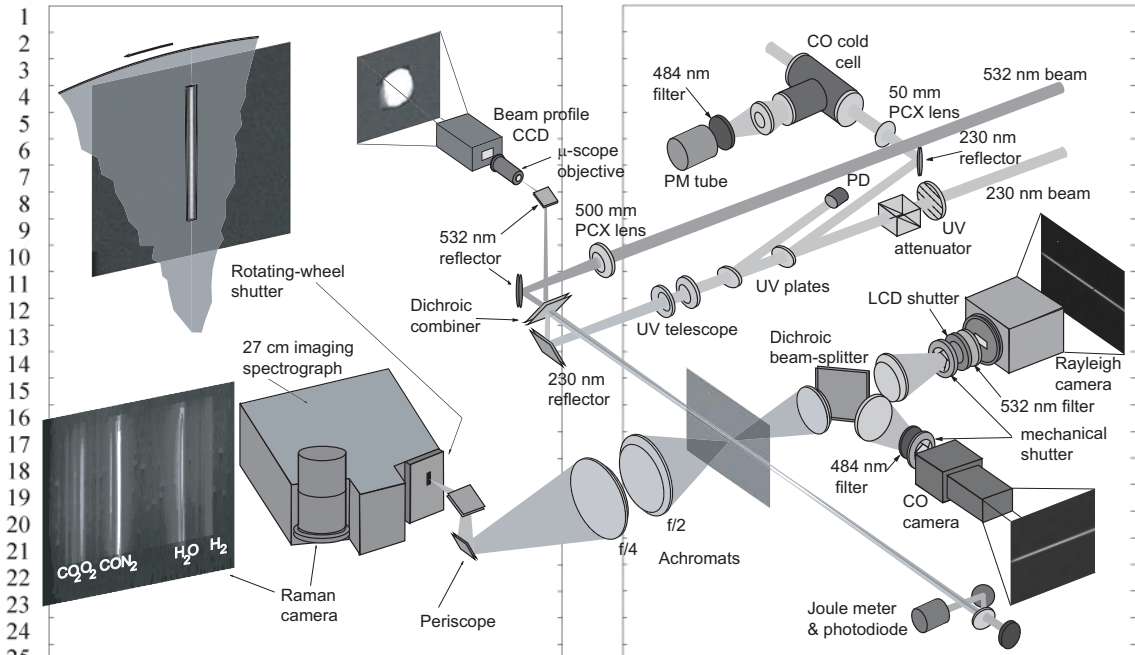


Fig. 1. Experimental system for simultaneous line imaging of Raman scattering, Rayleigh scattering, and CO LIF.

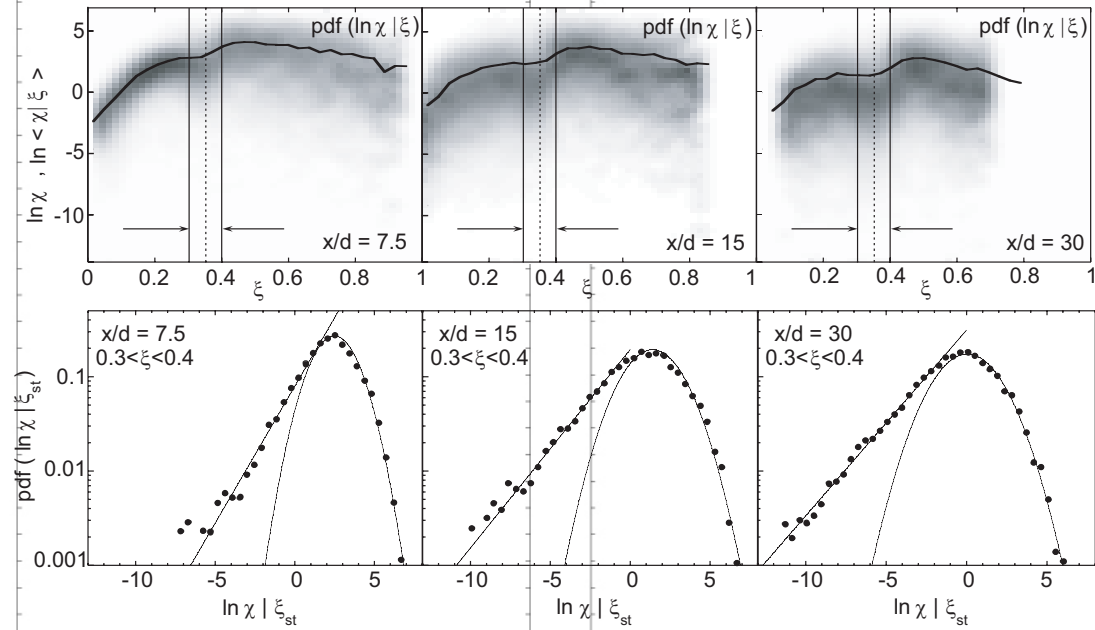
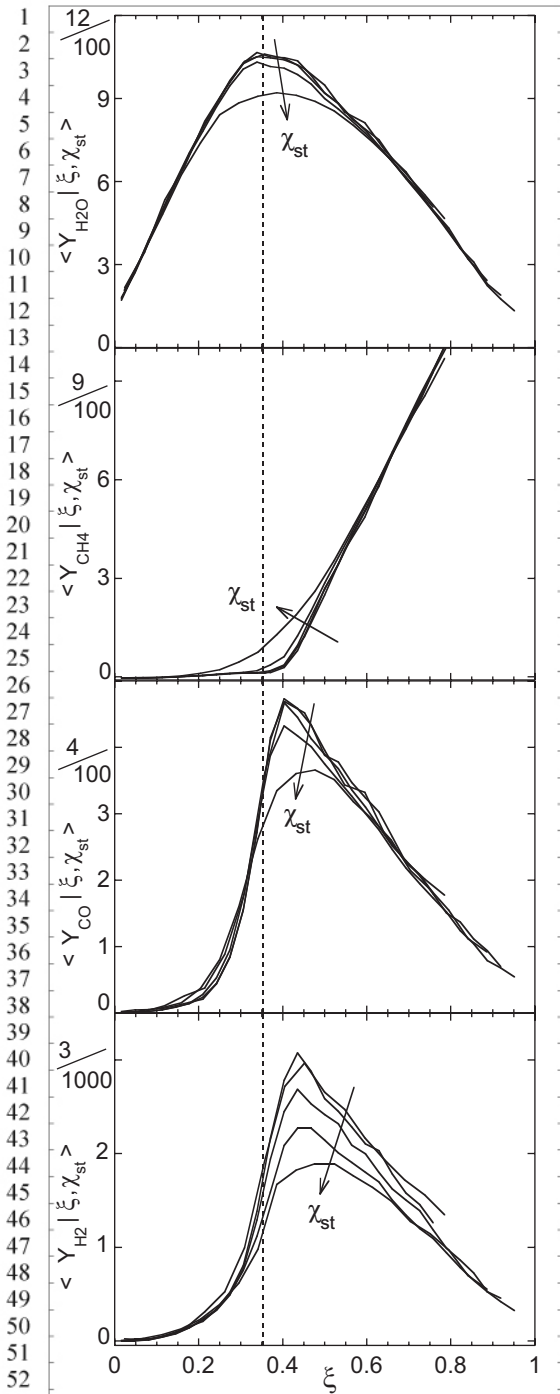


Fig. 2. Top row: density plots of scalar dissipation for the three axial positions ($x/d = 7.5, 15,$ and 30) in flame D. Darker areas correspond to higher density in the $pdf(\ln \chi | \xi)$. The average conditional scalar dissipation ($\ln \langle \chi | \xi \rangle$) is plotted as a solid line. Bottom row: 1D pdf of scalar dissipation conditioned upon the mixture fraction around the stoichiometric value ($pdf(\ln \chi | \xi_{st})$). Data within the range $0.3 \leq \xi \leq 0.4$ were used to form the 1D pdf s. Solid lines represent exponential and log-normal fits to the left and right tails of the pdf , respectively.

57 $x \times 2 = 114$ lines for Figs. 1, 2

61 Lines of 9 pt Times New Roman with 10 pt line spacing



54 Fig. 3. Average species mass fractions doubly
 55 conditioned on the local value of ξ and on the value of
 56 scalar dissipation at the nearest stoichiometric location, χ_{st} ,
 57 in each instantaneous profile. The five plotted lines
 58 correspond to five logarithmic intervals used for binning χ_{st} :
 59 0.01-0.1, 0.1-1, 1-10, 10-100, and 100-1000 (all values in s^{-1}).
 60 The arrows indicate increasing χ_{st} , and the dashed line
 61 shows the stoichiometric condition.

62
63
64
65
66
67
68
69
70
71
72
73
74
75
76
77
78
79
80
81
82
83
84
85
86
87
88
89
90
91
92
93
94
95
96
97
98
99
100
101
102
103
104
105
106
107
108
109
110
111
112
113
114
115
116
117
118
119
120
121
122

61 Lines of 9 pt Times New Roman with 10 pt line spacing

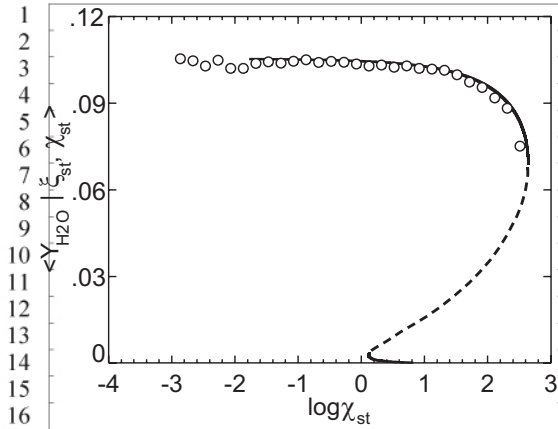


Fig. 4. Average water mass fraction doubly conditioned on stoichiometry (ξ_{st}) and on the local value of scalar dissipation χ_{st} . Line: S-shaped curve (mirrored) for extinction of single-step reaction (from [26]). Dashed portion corresponds to the unstable branch of the curve.

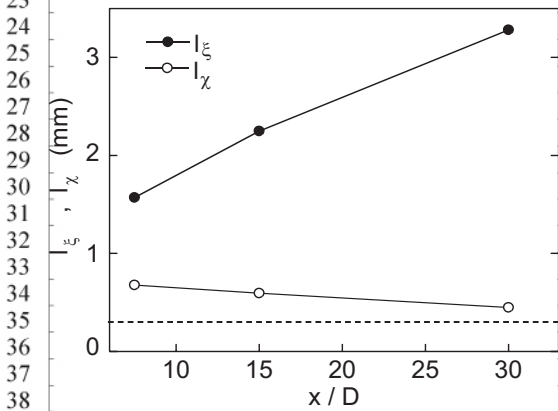


Fig. 5. Length scales of turbulent fluctuations in the mixture fraction (l_ξ) and scalar dissipation (l_χ) measured in flame D. The dashed line corresponds to the experimental resolution limit.

61 lines for Fig 3 + 44 lines for Figs 4, 5.

Total: 5 full pages plus...

(60+114 + 61 + 44) lines / (122 lines per page)

7.29 pages total length

62
63
64
65
66
67
68
69
70
71
72
73
74
75
76
77
78
79
80
81
82
83
84
85
86
87
88
89
90
91
92
93
94
95
96
97
98
99
100
101
102
103
104
105
106
107
108
109
110
111
112
113
114
115
116
117
118
119
120
121
122